Resilience-oriented Hardening and Expansion Planning of Transmission System Under Hurricane Impact

Jing Zhou, Heng Zhang, Haozhong Cheng, *Fellow*, *CSEE*, Shenxi Zhang, Lu Liu, Zheng Wang, and Xiaohu Zhang

***Abstract*—In this paper, we propose a two-stage transmission hardening and planning (TH&P) model that can meet the load growth demand of normal scenarios and the resilience requirements of hurricane-induced damage scenarios. To better measure the resilience requirements, the proposed TH&P model includes two resilience assessment indexes, namely, the load shedding (LS) under the damage scenario and the average connectivity degree (ACD) at different stages. The first-stage model, which aims to meet the load growth demand while minimizing the LS, is formulated as a mixed-integer linear program (MILP) to minimize the total planning and hardening cost of transmission lines, the operating cost of generators, and the penalty cost of wind power and load shedding in both normal and damage scenarios. The second-stage model aims to further improve the ACD when the ACD of the scheme obtained from the first-stage model cannot reach the target. Specifically, the contribution of each transmission line to the ACD is calculated, and the next hardened line is determined to increase the ACD. This process is repeated until the ACD meets the requirements. Case studies of the modified IEEE RTS-24 and two-area IEEE reliability test system-1996 indicate the proposed TH&P model can meet the requirements for both normal and damage scenarios.**

***Index Terms*—Hardening, hurricane disaster, resilience, transmission expansion planning.**

NOMENCLATURE

A. Set

$\Gamma, \Gamma^*, \Gamma^-$	Set of all lines, candidate lines, and existing lines, respectively.
$\Omega_{\rm NS}, \Omega_{\rm DS}$	Set of normal and damage scenarios, respectively.
$\Omega_{\rm H}, \Omega_{\rm H'}$	Set of duration of representative days in normal operating conditions and emergency operating conditions, respectively.
$\Omega_{\rm B}$	Set of all buses.
$\Omega_{\rm G}, \Omega_{\rm W}$	Set of wind farms and generators, respectively.

B. Parameters

$C_{h,l}, C_l$	Investment cost for hardening and constructing line l (\$).
C_g	Operating cost for generator g (\$/MWh).
$C_{ls,ns}$	Penalty cost for load shedding in normal and (\$/MWh).
$C_{ls,ds}$	Penalty cost for load shedding in damage scenarios (\$/MWh).
C_w	Wind curtailment penalty factor of wind farm w (\$/MWh).
q_{ns}, q_{ds}	Probabilities of normal scenario ns and damage scenario ds, respectively.
$\tau_{h,ns}, \tau_{h',ds}$	Duration of normal scenario ns and damage scenario ds, respectively.
$p_g^{\max}, p_g^{\min}$	Maximum and minimum capacity limit of generator g, respectively (MW).
$p_{w,s}^{\max}, p_{w,s}^{\min}$	Maximum and minimum output limit of wind farm w in scenario s, respectively (MW).
$p_{b,s}$	Power demand of bus b in scenario s (MW).
$p_l^{\max}$	Maximum capacity limit of line l (MW).
B_l	Admittance of line l.
$v_{l,s}$	Binary parameter to indicate whether line l is attacked ($v_{l,s}=0$) by a hurricane or not ($v_{l,s}=1$).
M	Big M is a large positive number.

C. Variables

h_l	The binary decision variable indicates whether line l is hardened ($h_l=1$) or not ($h_l=0$).
x_l	The binary decision variable indicates whether line l is constructed ($x_l=1$) or not ($x_l=0$).
$P_{g,s}$	The output power of generator g in scenario s (MW).
$p_{ls,b,s}$	Load curtailment of bus b in scenario s (MW).
$P_{w,s}$	The output power of wind farm w in scenario s (MW).
$P_{w,s}^{wc}$	Curtailed wind power of wind farm w in scenario s (MW).
$f_{l,s}$	Power flow in line l in scenario s (MW).
$\theta_{m(l),s}$, $\theta_{m(l),s}$	Voltage angle of bus m, n (connected to line l) in scenario s, respectively (rad).

Manuscript received October 25, 2022; revised March 11, 2023; accepted May 31, 2023. Date of online publication February 27, 2024; date of current version March 26, 2024. This work was sponsored by National Natural Science Foundation of China (U1966206, 51907123), Shanghai Sailing Program (20YF1418900), and State Grid Corporation of China (SGHD0000GHJS2200346).

J. Zhou, H. Zhang (corresponding author, email: zhangheng_sjtu@sjtu.edu.cn), H. Z. Cheng, S. X. Zhang, and L. Liu are with Key Laboratory of Control of Power Transmission and Conversion, Ministry of Education, Electrical Engineering Department, Shanghai Jiao Tong University, Shanghai 200240, China.

Z. Wang and X. H. Zhang are with State Grid East China Branch, Shanghai 200120, China.

DOI: 10.17775/CSEEJPES.2022.07300

I. Introduction

In recent years, natural disasters such as hurricanes, ice storms, and earthquakes have been increasing around the world [1]. Natural disasters often damage the components of a system and cause large-area blackouts, posing great challenges for the safe and reliable operation of power systems. For instance, in 2012, Hurricane Sandy hit the United States, causing economic losses of more than $60 billion and power outages for millions of people. In 2016, a hurricane hit Jiangsu Province, China, which tripped more than ten transmission lines and causing more than 100,000 customers to suffer power outages [2]. To mitigate the related risks of natural disasters, the concept of power system resilience, which means the ability to resist, absorb, accommodate and recover from the effects of a hazard, is presented [3]. Compared with reliability, resilience is faced with high-impact and low-probability (HILP) events and is tied to coping with one or more specific threats [4], and it exhibits dynamic behavior because of changes in network topology [5].

Based on different periods of the response of a power system to natural disasters, power system resilience enhancement strategies can be divided into three categories: 1) pre-disaster system hardening and planning [6]–[18]; 2) emergency response during the disaster [19]–[21]; and 3) restoration after the disaster [22]–[25]. Focusing on the pre-disaster stage of resilience enhancement of the transmission system, many studies have made useful achievements.

Hardening measures (HMs) enhance system resilience by strengthening transmission system components. Reference [6] adopted load shedding (LS) as a resilience assessment index (RAI) and applied HMs to minimize the LS under extreme weather events (EWEs). Reference [7] improved the resilience of an integrated electricity-gas system in case of an earthquake through HMs, while power and natural gas load loss (LL) were used to represent the integrated system's resilience. Reference [8] presented in-depth research on multiple types of natural disasters; expected LS (ELS) was utilized as an RAI, and HMs were used to improve this index. Reference [9] proposed a resilient attacker-defender planning model to improve the power system's resilience, while the LS and the number of damaged components were adopted as RAIs. Reference [10] proposed a novel comprehensive index framework to measure system resilience in terms of LS, transmission lines, and generation after EWEs; then, HMs and smart operational measures were utilized to develop the index. However, only using load-related RAIs (LRAIs) to quantify resilience, with less consideration given to assessing the disaster-induced damage to network structural integrity, will lead to a biased resilience assessment result. The reason is the result may ignore damage conditions with a small LS but severe structural degradation, leading to an underestimation of system structural damage and an inability to effectively provide advice on implementing HMs.

In addition to the application of HMs, planning measures (PMs) that enhance system resilience by constructing different transmission system devices are widely implemented. Reference [11] adopted worst-case expected load shedding (WCEL) as an RAI and proposed a planning model for transmission lines with optimal transmission switching to enhance system resilience under typhoon conditions. Reference [12] evaluated system resilience through LS and proposed a novel RAI from the perspective of capacity adequacy, namely, reachability (RA). Joint planning of PV generation and battery storage was conducted to improve these two indexes under EWEs. Reference [13] adopted LS as an RAI and proposed a novel resilience-based tri-level model for jointly planning transmission lines and substations to minimize the LS under EWEs. Reference [14] introduced deep learning into resilience studies and presented a co-planning model for transmission lines, battery energy storage and wind farms, and LS was utilized as an RAI and reduced through the proposed model. Reference [15] proposed a novel resiliency-oriented model considering both normal and damage scenarios, adopted the LS under EWEs as an RAI, and reduced it through the construction of transmission lines and distributed energy resources. However, PMs are long-term resilience enhancement measures (REMs), and this long-term period often contains numerous normal scenarios and relatively few hurricane-induced damage scenarios. Only implementing PMs to meet the resilience requirements of disaster-induced damage scenarios is uneconomical and not realistic.

A few papers [16]–[18] have studied the implementation of both HMs and PMs together to enhance resilience in addition to the utilization of hardening and planning measures separately. Reference [16] adopted the ELS under EWEs as an RAI and presented a novel transmission defense planning model to collaboratively construct and enhance transmission lines to further reduce the ELS. Reference [17] adopted the expected load reduction (ELR) as an RAI, and then, the HMs and PMs were selectively implemented to enhance system resilience through the cost-effectiveness ratio and construction difficulty. Reference [18] considered LL as an RAI and presented a resilient constrained planning model for the joint consideration of generators and hardening transmission lines to minimize LL under floods and earthquakes. However, implementing HMs and PMs in different stages can effectively enhance system resilience, but it cannot enable an economic scheme and cannot overcome shortcomings, namely, underestimating the degradation of the system structure and implementing PMs in an uneconomical way without considering the requirements of normal scenarios.

Table I summarizes the above references [6]–[18] in terms of natural disasters, RAI, REMs, and consideration of scenarios. In Table I, NS and DS are shorthand for a normal scenario and a damage scenario. Notably, LRAI contains relevant RAIs such as LS, LL, ELS, WCEL and ELR.

On the premises of the analysis above, the major research gaps are as follows: (1) Only adopting LRAIs cannot completely reflect damage to the network structure, which will lead to a biased resilience assessment result without considering structure-related RAIs (SRAIs). (2) Implementing PMs only aims to meet the resilience requirements of damage scenarios, which is uneconomical and not realistic. In addition, separately implementing PMs and HMs in different stages cannot enable optimal economic costs to be achieved for the scheme. The

main objective of this paper is thus to propose a collaborative transmission hardening and planning (TH&P) model to meet requirements of both normal and hurricane-induced damage scenarios.

The main contributions are as follows:

- To address research gap (1), this paper adopts the LS under damage scenarios and the average connectivity degree (ACD) as two RAIs to comprehensively measure transmission system resilience from the perspective of system loss and the overall connectivity status.
- To address research gap (2), this paper presents a TH&P model to collaboratively implement these two measures to meet load growth demand for normal scenarios and the resilience requirements for damage scenarios, simultaneously. In addition, considering the complexity of directly embedding the two RAIs into the same stage of the model, the proposed TH&P model is constructed in two stages to help these two RAIs reach their target values separately. Furthermore, this model can be effectively solved and extended to cover other RAIs that cannot be solved directly.

The rest of the paper is organized as follows:

Hierarchical structure is described in Section II. Section III introduces the hurricane simulation model and the formulation of the two RAIs. Section IV describes the mathematical formulation of the proposed TH&P model. Section V validates the proposed model on a modified IEEE RTS-24 and two-area IEEE RTS-1996. The conclusions are summarized in Section VI.

II. Hierarchical Structure

The objective of this paper is to develop an economical scheme while meeting the requirements of system resilience. Hence, a tractable two-stage mathematical model intended for TH&P problems is proposed to meet the requirements of normal and damage scenarios for a transmission system, and a hierarchical structure is illustrated in Fig. 1. For normal scenario considerations, the load growth demand needs to be met, and wind curtailment and LS should be avoided as much as possible. For damage scenario considerations, ability of the transmission system to resist damage from hurricanes needs to be quantified and improved.

TABLE I
Taxonomy of Recent Research Works

Section	Aspect	Reference number													
		[6]	[7]	[8]	[9]	[10]	[11]	[12]	[13]	[14]	[15]	[16]	[17]	[18]	TH&P model
Natural disasters	EWEs	√		√	√	√	√		√	√	√		√		√
	Others		√	√				√				√		√	
RAI	LRAI	LS	LL	ELS	LS	LS	WCEL	LS	LS	LS	LS	ELS	ELR	LL	LS
	SRAI							RA							ACD
REMs	HMs	√	√	√	√	√						√	√	√	√
	PMs						√	√	√	√	√	√	√	√	√
Scenario	DS	√	√	√	√	√	√	√	√	√	√	√	√	√	√
	NS										√				√

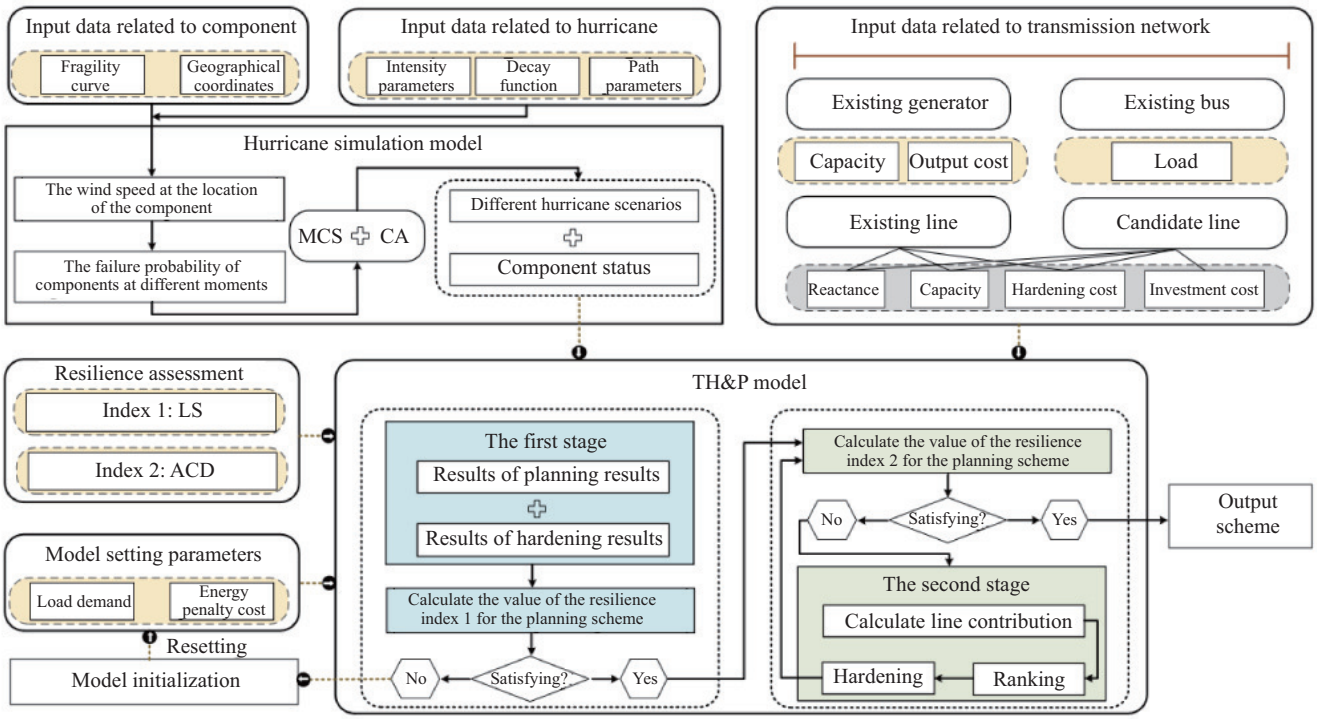

Fig. 1. The hierarchical structure of the proposed two-stage TH&P model.

Natural disaster events tend to destroy the network topology and weaken system resilience. Before enhancing resilience, quantification of resilience is a primary task. Ensuring load supply is a primary goal of the transmission system, and the quantity of the LS under hurricanes can visually quantify the adverse impact of hurricanes on the system and demonstrate the benefits of different REMs. Moreover, the LS is a widely used index in resilience studies. Therefore, this paper also adopts the LS as one of the RAIs. Additionally, using only the LS as a RAI cannot completely reflect hurricane-induced damage to the network structure and may lead to a biased resilience assessment result. The result may ignore damage conditions with a small LS but severe structural degradation and lead to an underestimation of system structure damage. Therefore, this paper adopts the ACD as another RAI.

Notably, there is no consensus on the most appropriate resilience indexes, and researchers choose the indexes based on their research needs.

After quantifying system resilience, resilience can be enhanced by HMs and PMs. To achieve a more resilient enhancement performance, two REMs are applied. However, HMs and PMs are determined separately in different stages and cannot obtain optimal economic costs for the scheme. In this paper, HMs are implemented in the planning stage to explore the advantages of combining these two measures in the same stages.

In reality, HMs include laying underground transmission lines, strengthening the transmission network components with more robust types of materials, and moving the transmission lines to places less influenced by severe climate-related events. PMs include adding new components and devices, such as transmission lines, energy storage, and generators. It seems that these two measures are very different in terms of their time scale.

However, the two measures can be implemented on the same time scale. For example, when new components for the transmission network need to be constructed to meet the requirements of load growth, considering the impact of hurricanes on the system, components with higher resilience can be prioritized for construction. Taking line construction as an example, underground transmission lines can be constructed instead of overground lines, and more robust materials can be used. By doing so, the HMs and PMs are implemented on the same time scale.

Based on the two RAIs, we need to implement HMs and PMs to reduce LS and increase the ACD based on economic considerations. To achieve this goal, LS is formed as a part of the objective function and is satisfied in the first stage of the proposed model, while the ACD reaches the target in the second stage through a repeated process.

Before using the proposed TH&P model, the impact of a hurricane on the transmission system's components, whether they are damaged or operating normally, needs to be determined. To achieve this goal, we establish a hurricane simulation model to generate real-time wind speed at the location of components and then obtain the failure probability of each component. To simulate different damage situations caused by a hurricane, Monte Carlo simulation (MCS) is used to determine the final state of the components and generate a large number of damage scenarios. However, considering all these scenarios in the proposed TH&P model is not realistic and uneconomical. Hence, a clustering algorithm (CA) is adopted to transform the massive scenarios into typical scenarios.

III. Hurricane Simulation Model

In this section, a hurricane simulation model is utilized to generate the wind speed at the location of each component. Then, the failure probability of different components at different times is calculated based on wind speed. The detailed process of generating hurricane-induced damage scenarios is described, and two RAIs are introduced.

A. Hurricane simulation

To quantify impact of hurricanes on transmission network components at different moments, a Batts hurricane model [26] is adopted to simulate the changing process of a hurricane. The Batts model is a mature wind field model that assumes decay in hurricane intensity over time is caused by a reduction in the central pressure difference. The moving path of a certain hurricane is shown in Fig. 2.

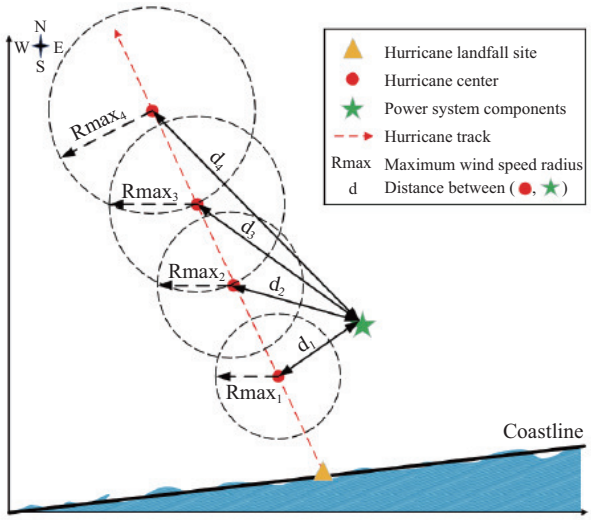

Fig. 2. The moving path of a certain hurricane.

A related parameter, central pressure difference $\Delta p(t)$, and the maximum wind speed radius of the hurricane $R_{\max}(t)$ are expressed as follows [27]:

$$\Delta p(t) = p_a - p_{\mathrm{ty}}(t) \tag{1}$$

$$\Delta p(t) = \Delta p(t_{\mathrm{land}}) \mathrm{e}^{(-\alpha(t-t_{\mathrm{land}}))} \quad t > t_{\mathrm{land}} \tag{2}$$

$$\alpha = \beta + \chi \left(\frac{\Delta p(t_{\mathrm{land}}) v_{\mathrm{H}}(t_{\mathrm{land}})}{R_{\max}(t_{\mathrm{land}})} \right) \tag{3}$$

$$R_{\max}(t) = \mathrm{e}^{(\xi - \eta \times 10^{-5} \Delta p(t)^2)} \tag{4}$$

where p_a (mb) represents the ambient pressure, which is a constant parameter (1013 mb). $p_{\mathrm{ty}}(t)$ represents the central hurricane pressure. t_{land} represents the time when the hurricane makes landfall. α, β, χ, ξ and η are the coefficient

parameters. $v_{\mathrm{H}}(t_{\mathrm{land}})$ (m·s^{-1}) represents the translation speed of the hurricane at time t_{land}.

Based on the central pressure difference $\Delta p(t)$, wind speed at the component location $v_{\mathrm{com}}(t)$ can be obtained by:

$$v_g^{\max}(t) = k\sqrt{\Delta p(t)} \tag{5}$$

$$v_t^{\max}(t) = \delta v_g^{\max}(t) + \varepsilon v_{\mathrm{H}}(t) \tag{6}$$

$$v_{\mathrm{com}}(t) = \begin{cases} v_t^{\max}(t) \times d(t)/R_{\max}(t) & d(t) \le R_{\max}(t) \\ v_t^{\max}(t) \times (R_{\max}(t)/d(t))^{0.6} & d(t) > R_{\max}(t) \end{cases} \tag{7}$$

where k, δ and ε represent the coefficients. $v_t^{\max}(t)$ represents the maximum wind speed at time t. $d(t)$ represents the distance between the hurricane center and the component position at time t and can be obtained by (8)–(10):

$$d(t) = ((x_{\mathrm{com}} - x(t)) + (y_{\mathrm{com}} - y(t)))^{0.5} \tag{8}$$

$$x(t) = x_{\mathrm{land}} + v_{\mathrm{H}}(t) t \cos\varphi \tag{9}$$

$$y(t) = y_{\mathrm{land}} + v_{\mathrm{H}}(t) t \cos\varphi \tag{10}$$

where $(x_{\mathrm{com}}, y_{\mathrm{com}})$, $(x(t), y(t))$ and $(x_{\mathrm{land}}, y_{\mathrm{land}})$ represent geographical coordinates of the component, the hurricane center at time t and at time t_{land}, respectively.φ is the angle between the hurricane path and coastline.

B. Component Failure Model

Transmission corridors are more likely to be damaged by extreme wind speeds from hurricanes, while transformers and cables are virtually unaffected [28], [29]. Therefore, when analyzing the impact of hurricanes on a transmission system, we only focus on the damage to transmission lines. To consider different wind speeds in different segments of the transmission corridor, a long transmission corridor can be considered as a series of transmission line segments connected by transmission towers.

1) Failure Model of Towers and Line Segments

Previous research has constructed wind fragility curves for components from real data. This model can reflect failure probability of components under different wind speeds and is widely used in resilience studies. Here, the prescribed analytical fragility function [30] based on structural characteristics is adopted to assess the probability of tower collapse under hurricanes. Cumulative failure probability of each tower in duration T is indicated as [30]:

$$\mu_m^k(t_i) = \begin{cases} 0 & v_m^k(t_i) \in [0, v_{\mathrm{tower}}^{\mathrm{des}}] \\ \mathrm{e}^{\gamma\left[v_m^k(t_i) - 2v_{\mathrm{tower}}^{\mathrm{des}}\right]} & v_m^k(t_i) \in (v_{\mathrm{tower}}^{\mathrm{des}}, 2v_{\mathrm{tower}}^{\mathrm{des}}) \\ 1 & v_m^k(t_i) \in [2v_{\mathrm{tower}}^{\mathrm{des}}, \infty) \end{cases} \tag{11}$$

$$p_m^k = 1 - \exp\left\{ - \sum_{i=0}^{N-1} \frac{\mu_m^k(t_i)}{1 - \mu_m^k(t_i)} \Delta t \right\} \tag{12}$$

where the combination of the superscript and subscript (m, k) represents the kth tower of the mth transmission corridor. For each tower, $\mu_m^k(t_i)$ is the failure rate at time t, $v_m^k(t_i)$ is the wind speed at time t, γ is the shape factor, and $v_{\mathrm{tower}}^{\mathrm{des}}$ is the design wind speed. N is the total number of shorter divided periods, and Δt is the time interval of each period.

All points on the line segment between two adjacent towers are assumed to be affected by the same wind speed. Similarly, the cumulative failure probability of each line segment in duration T is indicated as [30], [31]:

$$\mu_m^l(t_i) = \exp\left[\varsigma \times \frac{v_m^l(t_i)}{v_{\mathrm{line}}^{\mathrm{des}}} - \rho \right] \Delta l \tag{13}$$

$$p_m^l = 1 - \exp\left\{ - \sum_{i=0}^{N-1} p_m^l(t_i) \Delta t \right\} \tag{14}$$

where the combination of the superscript and subscript (m, l) represents the lth line segment of the mth transmission corridor. For each line segment, $\mu_m^l(t_i)$ is failure rate at time t, and ς and ρ are parameter coefficients. $v_m^l(t_i)$ is the wind speed at time t, $v_{\mathrm{line}}^{\mathrm{des}}$ is the design wind speed, and Δl is the length of the line segment between two adjacent towers.

2) Failure Model of a Transmission Corridor

Since a long transmission corridor is considered to be a series of transmission towers connected to line segments, the equivalent failure probability of a transmission corridor can be expressed as follows:

$$P_m = 1 - \prod_1^K (1 - p_m^k) \prod_1^L (1 - p_m^l) \tag{15}$$

where K and L represent total number of transmission towers and line segments for the mth transmission corridor, respectively.

C. Hurricane Damage Scenario Generation Process

In general, the process of generating hurricane damage scenarios is as follows:

Step 1) Input Data

The hurricane and system component data are input. Hurricane data include the translation speed, moving direction, and central pressure difference when the hurricane makes landfall. Transmission system component data include the geographic coordinates of each bus and the fragility curves of the towers and line segments.

Step 2) Hurricane Simulation

The total hurricane-affected period T is determined, and the total period T is divided into equal time intervals. In each time interval $[t_k, t_{k+1}]$, wind speed at the location of each tower and line segment is assumed to be constant. Then, the distances between the hurricane center and component locations are calculated with (8)–(10). Next, the changes in hurricane intensity and wind speeds at all component locations are calculated with (1)–(4) and (5)–(7), respectively. Then, the cumulative failure probabilities of the towers and line segments are calculated to obtain the failure probability of the corresponding lines with (11)–(15).

Step 3) Typical Damage Scenario Generation

After obtaining the failure probabilities of all lines at time intervals $[t_k, t_{k+1}]$, Monte Carlo simulation is used to determine final state of each line [32]. When all component states in time interval $[t_k, t_{k+1}]$ are obtained and the next time interval is reached, steps (2)–(3) are repeated until the total period is complete. Then, component states at time t_n

are recorded to generate a damage scenario. In this paper, a total of 2000 sampled damage scenarios are generated and transformed into 4 typical damage scenarios by the k-means cluster algorithm.

D. Resilience Assessment Index

Hurricanes can cause the disconnection of multiple corridors in the transmission system, weakening transmission function and resulting in a LS. To reflect the degradation in system performance caused by hurricanes, an index widely used in previous studies [6]–[15], namely, the LS, is adopted.

(1) Transmission system load shedding (LS)

$$\mathrm{LS} = \sum_{ds\in\Omega_{\mathrm{DS}}} q_{ds} \sum_{b\in\Omega_{\mathrm{B}}} p_{ls,b,ds} \tag{16}$$

where LS represents the total load shedding of the transmission system under hurricane-induced damage scenarios. q_{ds} represents the probability of each damage scenario. $p_{ls,b,ds}$ represents the load shedding at bus b under damage scenarios.

The LS is a widely used index in resilience studies that can visually quantify the adverse impact of hurricanes on the system and demonstrate the benefits of different REMs.

(2) Average connectivity degree

Using only LS cannot completely reflect the damage to the network structure and may lead to a biased resilience assessment result. The result may ignore damage conditions with a small LS but severe structural degradation and lead to an underestimation of system structural damage. Therefore, another index, the ACD, is adopted to consider the overall system connectivity status:

$$\mathrm{ACD} = \sum_{ds\in\Omega_{\mathrm{DS}}} q_{ds} \left(\frac{\mathrm{CI}_{k-m}^{ds}}{\mathrm{N}(k,m)} \right) \tag{17}$$

where ACD represents the average connectivity of all generator nodes and load nodes of the system under the damage scenario. CI_{k-m}^{ds} represents the connectivity degree between generator k and load node m under damage scenario ds. If generator k and load node m remain on the same island under damage scenario ds, then CI_{k-m}^{ds} equals 1. Otherwise, CI_{k-m}^{ds} equals 0. $\mathrm{N}(k,m)$ represents the total number of generator–node pairs in the initial system.

IV. Problem Formulation

The model of this paper is obtained to develop an economical scheme while meeting requirements of system resilience. This paper adopts LS under damage scenarios and the ACD as two RAIs to quantify hurricane stress on the network. Then, a cost-optimal objective function is set to meet the requirements of the two RAIs so an economic planning solution can be obtained to reduce the impact of hurricanes. Based on the two RAIs proposed in the previous section, a two-stage TH&P model is proposed in this section to reduce the LS while increasing the ACD of the transmission system and ultimately improving system resilience. To achieve this goal, LS is formed as a part of the objective function of the first-stage model, as shown in (18), while the ACD reaches the target in the second stage through a repeated process.

A. Model formulation

(1) First-stage model

$$\min \quad \mathrm{TC} = \mathrm{HPC} + \mathrm{NSC} + \mathrm{DSC} \tag{18}$$

$$\mathrm{HPC} = \sum_{l\in\Gamma} c_{h,l} h_l + \sum_{l\in\Gamma*} c_l x_l \tag{18a}$$

$$\mathrm{NSC} = \sum_{ns\in\Omega_{\mathrm{NS}}} q_{ns} \sum_{h\in\Omega_{\mathrm{H}}} \tau_{h,ns} \Bigg(\sum_{g\in\Omega_{\mathrm{G}}} c_g P_{g,ns} + \sum_{b\in\Omega_{\mathrm{B}}} c_{ls,ns} p_{ls,b,ns} + \sum_{w\in\Omega_{\mathrm{W}}} c_w (P_{w,ns}^{\max} - P_{w,ns}^{wc}) \Bigg) \tag{18b}$$

$$\mathrm{DSC} = \sum_{ds\in\Omega_{\mathrm{DS}}} q_{ds} \sum_{h'\in\Omega_{\mathrm{H}'}} \tau_{h',ds} \Bigg(\sum_{g\in\Omega_{\mathrm{G}}} c_g P_{g,ds} + \sum_{b\in\Omega_{\mathrm{B}}} c_{ls,ds} p_{ls,b,ds} \Bigg) \tag{18c}$$

The objective function (18) consists of three parts, (18a)–(18c). HPC in (18a) represents the total investment cost, which includes the line hardening cost and construction cost. NSC in (18b) represents total cost (TC) of normal scenarios, where the first part represents the operating costs (OCs) of thermal generators and the second and third parts represent the LS and wind curtailment penalties under normal scenarios, respectively. DSC in (18c) represents the TC of damage scenarios, and the two parts represent the OCs of thermal generators and LS under damage scenarios. To reduce LS, a large value of $c_{ls,ds}$ is adopted to ensure value of $p_{ls,b,ds}$ is as small as possible in the final resilience enhancement scheme. On this basis, to minimize the TC during the model solving process, LS with a large penalty cost coefficient ($c_{ls,ds} p_{ls,b,ds}$) will be reduced as small as possible, and the goal of LS reduction is achieved.

$$\sum_{g\in\Omega_{\mathrm{G}}} P_{g,s} + \sum_{w\in\Omega_{\mathrm{W}}} (P_{w,s}^{\max} - P_{w,s}^{wc}) + \sum_{l\in L^+(b)} f_{l,s} - \sum_{l\in L^-(b)} f_{l,s} = \sum_{b\in\Omega_{\mathrm{b}}} (p_{b,s} - p_{ls,b,s}) \quad \forall b \in \Omega_{\mathrm{B}} \tag{19}$$

$$P_g^{\min} \le P_{g,s} \le P_g^{\max} \quad \forall g \in \Omega_{\mathrm{G}} \tag{20}$$

$$P_{w,s}^{\min} \le P_{w,s}^{wc} \le P_{w,s}^{\max} \quad \forall w \in \Omega_{\mathrm{W}} \tag{21}$$

$$0 \le p_{ls,b,s} \le p_{b,s} \quad \forall b \in \Omega_{\mathrm{B}} \tag{22}$$

Constraint (19) represents the power balance for each bus. $L^+(b), L^-(b)$ are the sets of lines through which power flows into and out of bus b. Constraints (20)–(22) limit the value of thermal power generation, wind power generation and LS for each bus within a certain range. Note constraints (19)–(22) should be satisfied in both normal and damage scenarios, which means $\forall (s \in \Omega_{\mathrm{NS}} \cup \Omega_{\mathrm{DS}})$.

$$x_l \in \{0,1\} \quad l \in \Gamma* \tag{23}$$

$$h_l \in \{0,1\} \quad l \in \Gamma \tag{24}$$

$$h_l \le x_l \quad l \in \Gamma* \tag{25}$$

Constraints (23)–(24) indicate x_l and h_l are binary variables. $x_l = 1$ means line l is constructed; otherwise, line l is not constructed. Similarly, $h_l = 1$ means line l is

hardened; otherwise, line l is not hardened. In practice, hardening transmission lines does not completely avoid the danger from hurricanes, but it can significantly reduce the probability of hurricane-induced failures to a very small level. In this paper, we ignore the small probability of failure after the implementation of HMs and assume hardened lines are not disturbed by a hurricane. Constraint (25) is a logical constraint, indicating if line l is not constructed ($x_l = 0$), then line l cannot be hardened ($h_l = 0$).

$$(h_l + v_{l,s} - h_l v_{l,s})(\theta_{m(l),s} - \theta_{n(l),s}) = \frac{f_{l,s}}{B_l} \quad \forall l \in \Gamma^- \tag{26}$$

$$|f_{l,s}| \le P_l^{\max}(h_l + v_{l,s} - h_l v_{l,s}) \quad \forall l \in \Gamma^- \tag{27}$$

$$x_l(h_l + v_{l,s} - h_l v_{l,s})(\theta_{m(l),s} - \theta_{n(l),s}) = \frac{f_{l,s}}{B_l} \quad \forall l \in \Gamma* \tag{28}$$

$$|f_{l,s}| \le P_l^{\max} x_l(h_l + v_{l,s} - h_l v_{l,s}) \quad \forall l \in \Gamma* \tag{29}$$

Constraints (26)–(27) represent the power flow in terms of the phase angle and the line flow capacity limit of existing lines. Similarly, constraints (28)–(29) represent the same limitation for candidate lines. In constraints (26)–(29), the term $(h_l + v_{l,s} - h_l v_{l,s})$ ensures power flow constraints depend on a combination of hardening and hurricane disturbance. Note constraints (26)–(29) should be satisfied in both normal and damage scenarios, which means $\forall(s \in \Omega_{\mathrm{NS}} \cup \Omega_{\mathrm{DS}})$.

In normal scenarios ($s \in \Omega_{\mathrm{DS}}$), hurricanes do not have any impact on the transmission system. Thus, none of the transmission lines will be disconnected due to the hurricane. Therefore, $(v_{l,s} = 1)$ and $(h_l + v_{l,s} - h_l v_{l,s}) = 1$, and constraints (26)–(29) hold. In damage scenarios ($s \in \Omega_{\mathrm{DS}}$), after completing the hurricane simulation, the value $v_{l,s}$ is determined as input data to the model. If line l is not affected by a hurricane ($v_{l,s} = 1$), then $(h_l + v_{l,s} - h_l v_{l,s}) = 1$, and this situation can be regarded as a normal scenario. If line l is affected by a hurricane ($v_{l,s} = 0$), then $(h_l + v_{l,s} - h_l v_{l,s}) = h_l$, and the normal operation of line l at this time depends on whether HMs are taken. If line l is hardened ($h_l = 1$), line l can operate normally, and constraints (26)–(29) hold. If line l is not hardened ($h_l = 0$), then there is no power flow on line l, and constraints (26)–(29) hold.

Note constraints (26) and (28)–(29) are nonlinear, which can make the model difficult to directly solve. Therefore, the big-M method is adopted to linearize constraints (26), and the transformed expression is as follows:

$$|f_{l,s} - B_l(\theta_{m(l),s} - \theta_{n(l),s})| \le M(1 - (h_l + v_{l,s} - h_l v_{l,s})) \tag{30}$$

where M is a very large constant. To linearize constraints (28), the big-M method is first used, and the transformed expression is as follows:

$$|f_{l,s} - B_l(\theta_{m(l),s} - \theta_{n(l),s})| \le M(1 - x_l(h_l + v_{l,s} - h_l v_{l,s})) \tag{31}$$

Then, we rewrite constraint (31) as:

$$\begin{aligned} &|f_{l,s} - B_l(\theta_{m(l),s} - \theta_{n(l),s})| \\ &\le M(1 - (x_l h_l(1 - v_{l,s}) + x_l v_{l,s})) \end{aligned} \tag{32}$$

Then, to linearize the term $x_l h_l$ in constraints (32), we introduce the auxiliary binary variable $u_l = x_l h_l$:

$$|f_{l,s} - B_l(\theta_{m(l),s} - \theta_{n(l),s})| \le M(1 - (u_l - u_l v_{l,s} + x_l v_{l,s})) \tag{33}$$

$$\begin{cases} u_l \le x_l \\ u_l \le h_l \\ u_l \ge x_l + h_l - 1 \end{cases} \tag{34}$$

Similarly, the transformed expression of constraint (29) is as follows:

$$|f_{l,s}| \le P_l^{\max}(u_l - u_l v_{l,s} + x_l v_{l,s}) \tag{35}$$

In summary, the first stage of the TH&P model is composed of objective function (18) and constraints (19)–(25), (27), (30), and (33)–(35). By solving the first-stage model, we can obtain a hardening and planning scheme (abbreviated as PSH_0) that satisfies the LS requirement.

(2) Second-stage model

To increase the ACD, we formulated a second-stage model to address a situation in which the ACD of the planning scheme of the first-stage model cannot meet the requirements. If ACD has been satisfied, then the scheme is output, and the program is terminated. Otherwise, the contribution of each transmission line to the ACD is computed through (36):

$$\mathrm{RC}_l^{\mathrm{ACD}} = \mathrm{ACD}|_{\mathrm{PSH}_i \cup (h_l = 1)} - \mathrm{ACD}_{\mathrm{PSH}_i} \quad l \in \Xi \tag{36}$$

where $\mathrm{ACD}_{\mathrm{PSH}_i}$ represents the value of the ACD of the scheme PSH_i, and $(i = 0)$ means the first time the first-stage model is solved. $\mathrm{ACD}|_{\mathrm{PSH}_i \cup (h_l = 1)}$ represents the value of the ACD when line l is assumed to be hardened during a hurricane. $\mathrm{RC}_l^{\mathrm{ACD}}$ represents the percentage improvement in the ACD when line l is assumed to be 100% reliable during hurricane simulations. Ξ represents the set of lines not hardened. After the $\mathrm{RC}_l^{\mathrm{ACD}}$ values for all nonhardened lines are calculated, the line with the largest $\mathrm{RC}_l^{\mathrm{ACD}}$ is hardened to improve the value of the ACD. This process is repeated until the ACD meets the target value and the goal of increasing the ACD is achieved.

B. The Solution Process of The Proposed Model

The whole process of the TH&P model is shown in Fig. 3, and the main procedure is divided into 4 steps:

Step 1: Input related data, including the transmission network data and hurricane-induced damage scenarios. The first part includes the cost and capacity of generators, the hardening cost and capacity of both candidates and existing lines, and the load demand of each bus. Additionally, hurricane-induced damage scenarios with different corridor states are obtained through a hurricane simulation model. Move to step 2.

Step 2: Solve the first-stage model to obtain a hardening and planning scheme that satisfies the load growth demand. Then, calculate the value of the load supplied proportion (V[LSP]) of the obtained scheme based on the LS of PSH_0. If V[LSP] is less than or equal to the set target value ϑ_1, return to step 1 and reset the parameters. Otherwise, move to step 3.

Step 3: Calculate the value of the ACD (V[ACD]) for PSH_0 and compare this value with ϑ_2. If V[ACD] is less than

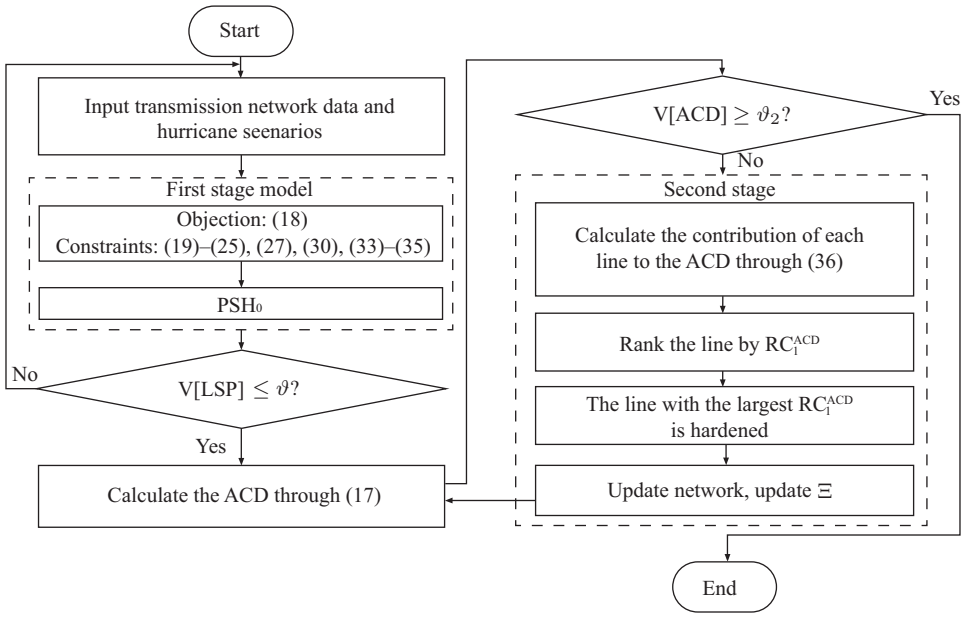

Fig. 3. The whole process of the TH&P model.

ϑ_2, then the ACD needs to be improved, and the second-stage model is initialized; move to step 4. Otherwise, stop the process and output the scheme.

Step 4: Solve the second-stage model to help V[ACD] reach the target. Contribution $\mathrm{RC}_l^{\mathrm{ACD}}$ of each nonhardened line ($l \in \Xi$) to the ACD is calculated and ranked. Then, the line with largest $\mathrm{RC}_l^{\mathrm{ACD}}$ is determined to be hardened. Update the scheme ($\mathrm{PSH}_0 \rightarrow \mathrm{PSH}_i$) and the set Ξ, and return to step 3.

V. Case Study

The proposed TH&P model is implemented on the modified IEEE RTS-24 [33] and the two-area IEEE RTS-1996 [34] under two simulated hurricanes. All programming is completed in MATLAB R2017a, and numerical results are obtained using the YALMIP toolbox and GUROBI solver on an individual computer with an i5 Intel Core and 8 GB RAM.

The meanings of abbreviations in this section are summarized in Table II. Two simulated hurricanes are considered for the resilience study, and the corresponding parameters are summarized in Table III. In general, parameters $\Delta p(t_{\mathrm{land}})$ and $\varphi(t_{\mathrm{land}})$ are assumed to conform to a log-normal distribution and normal distribution, respectively. The corresponding probability distribution curve can be obtained from reference [32], and then, the Monte Carlo method is adopted to obtain the initial values. In addition, the value of $V_{\mathrm{H}}(t_{\mathrm{land}})$ is taken to be consistent with reference [32].

Figure 4 shows a geographical location map of the IEEE RTS-24, and the detailed information refers to [32]. In practice, depending on the purpose of the application, the initial hurricane conditions can be replaced flexibly based on forecast data or historical data.

The other parameters in the hurricane simulation model are set as follows: β and χ in (3) are set to 0.006 and 0.00046, respectively [35]. ξ and η in (4) are set to 3.859 and 7.7, respectively [32]. k in (5) is set to 6.93 [30]. δ and ε in (6) are set to 0.865 and 0.5, respectively [30]. γ in (11) is set to 0.3 [36]. ς and ρ in (13) are set to 11 and 18, respectively [31]. $v_{\mathrm{tower}}^{\mathrm{des}}$ in (13) and $v_{\mathrm{line}}^{\mathrm{des}}$ in (11) are set to 35 m/s and 30 m/s, respectively [37].

The impact of two simulated hurricanes on the system was simulated approximately 2000 times and generated 2000 corresponding damage scenarios, which can include most situations of hurricane impact on the system in this region. In practical applications, historical hurricane data can be adopted as a supplement to enhance the practicality of the proposed model. Then, total damage scenarios are transformed into 4 typical damage scenarios by the k-means cluster algorithm. The states of the corridor under each typical damage scenario are introduced in Table IV.

TABLE II
Meaning of The Abbreviations in Section V

Abbreviation	Meaning	Unit
$\mathrm{C_{num}}$	Corridor number	–
fb, tb	From bus, to bus	–
PC	Planning cost	M$
HC	Hardening costs	M$
OC	Operation cost	M$
LSC	Load shedding cost	M$
TC	Total cost	M$
V[LSP]	Value of load supplied proportion	%
V[ACD]	Value of ACD	%

TABLE III
Data of Two Simulated Hurricanes

Aspect	Hurricane 1	Hurricane 2
$\Delta p(t_{\mathrm{land}})$	40 hPa	45 hPa
$V_{\mathrm{H}}(t_{\mathrm{land}})$	27 km/h	27 km/h
$\varphi(t_{\mathrm{land}})$	60°	90°

A. Modified IEEE RTS-24

The modified IEEE 24-RTS is adopted to demonstrate the effectiveness of the proposed TH&P model. The original case

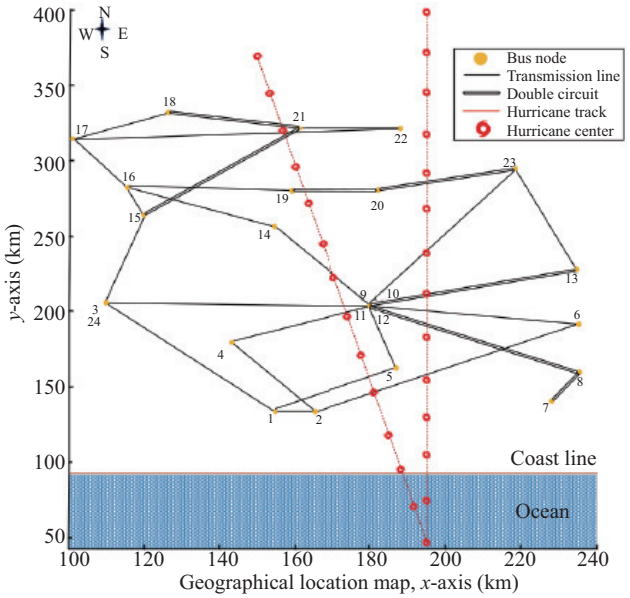

Fig. 4. IEEE RTS-24 under two simulated hurricanes.

TABLE IV
TYPICAL DAMAGE SCENARIOS FOR IEEE RTS-24

C_{num}	fb	tb	State 1	2	3	4	C_{num}	fb	tb	State 1	2	3	4
1	1	2				⋆	19	11	13			⋆	⋆
2	1	3	⋆	⋆	⋆	⋆	20	11	14	⋆		⋆	⋆
3	1	5			⋆	⋆	21	12	13	⋆	⋆	⋆	⋆
4	2	4	⋆		⋆	⋆	22	12	23	⋆	⋆	⋆	⋆
5	2	6	⋆	⋆	⋆	⋆	23	13	23			⋆	⋆
6	3	9	⋆		⋆	⋆	24	14	16				
7	3	24					25	15	16				
8	4	9		⋆	⋆	⋆	26+27	15	21			⋆	
9	5	10	⋆		⋆	⋆	28	15	24				
10	6	10	⋆		⋆	⋆	29	16	17				
11+12	7	8			⋆	⋆	30	16	19				
13	8	9	⋆	⋆	⋆	⋆	31	17	18				
14	8	10	⋆	⋆	⋆	⋆	32	17	22				
15	9	11					33+34	18	21				⋆
16	9	12					35+36	19	20				
17	10	11					37+38	20	23				
18	10	12					39	21	22				

⋆ indicates that a corridor is damaged under the damage scenarios.

contains 34 transmission corridors, and total load and generator capacity are 2850 MW and 3405 MW, respectively. Then, the thermal power capacity and load demand are increased to 1.5 times their original values to simulate the target of the planning year, and line capacity is reduced to 0.7 times its original value. The original values of thermal power capacity, load demand and line capacity can be found in [33]. The penalty costs of LS and curtailed wind energy are \$5000/MWh and \$150/MWh [38].

Corridor 7–8 adds a new line to ensure the system meets the $N-1$ criterion. Three wind farms are connected at buses 5, 8 and 19 with an initial capacity of 800 MW, and four representative days from reference [39] are taken as normal scenarios.

Two cases are designed to demonstrate the effectiveness of the TH&P model, and the descriptions are as follows:

Case 1 (C1): Collaborative implementation of HMs and PMs, considering normal and damage scenarios and adopting only the LS as an RAI, which is used in references [16], [18].

Case 2 (C2): Separate implementation of HMs and PMs, considering normal and damage scenarios and adopting only the ACD as an RAI.

Case 3 (C3): Separate implementation of HMs and PMs, considering normal and damage scenarios, and adopting two RAIs, namely, the LS and ACD.

TH&P: Collaborative implementation of HMs and PMs, considering normal and damage scenarios and adopting two RAIs, namely, the LS and ACD.

1) The Validity of The TH&P Model in Meeting The Requirements of The Two RAIs

To address the research gap stemming from the fact that quantitative RAIs are not fully used in terms of the overall network structure, this paper adopts the LS and ACD as two RAIs. To illustrate the validity and advantages of the proposed TH&P model for meeting the two RAIs' requirements, a comparison case (C1) is used. Planning results are presented in Table V.

TABLE V
PLANNING SCHEMES OF THE IEEE RTS-24 SYSTEM

Aspect	TH&P	C1	C2
PC (M\$)	179.4	179.4	158.2
HC (M\$)	851.9	591.9	771.9
OC (M\$)	1907.6	1907.6	2606.5
LSC (M\$)	0	0	92.2
TC (M\$)	2938.9	2678.9	3628.8
V[LSP] (%)	100	100	97.5
V[ACD] (%)	100	79.4	100

In Table V, V[LSP] represents value of the load supplied proportion based on the LS; a larger V[LSP] indicates a smaller LS and a better system resilience performance. It can be calculated as follows:

$$\mathrm{V[LSP]} = \frac{\sum_{ds\in\Omega_{\mathrm{DS}}} q_{ds} \sum_{b\in\Omega_{\mathrm{B}}} p_{b,s} - \mathrm{LS}}{\sum_{ds\in\Omega_{\mathrm{DS}}} q_{ds} \sum_{b\in\Omega_{\mathrm{B}}} p_{b,s}} \tag{37}$$

We observe from Table V C1 can make V[LSP] reach 100% and V[ACD] reach 79.4% with a TC of \$2678.9 M, while C2 can obtain 97.5% and 100% of the two aspects with a TC of \$3628.8 M, and the proposed TH&P model can achieve 100% values of the two aspects with a TC of \$2938.9 M.

Compared with C1, the TC of the TH&P model increases by approximately 9.7% due to the cost of additional hardened lines, and V[ACD] increases by 20.6% and meets the requirements (in this paper, V[ACD] needs to be 100%; in practice, different V[ACD] values can be set based on different situations). Compared with C2, the TC of the TH&P model is reduced by approximately 19%, and the V[LSP] of the TH&P model increases by approximately 2.5%. Because the scheme that only aims at improving the V[ACD] could not obtain a reasonable network structure, this will lead to inefficient and uneconomical power transmission and finally result in LS and an increment in generation costs. These results illustrate the proposed TH&P model can effectively meet the requirements of both RAIs with a certain cost increment compared to the case that only considers LS and has economic advantages in

terms of the TC compared to the case only considering the ACD. The specific resilience enhancement scheme is shown in the appendix.

2) The Effectiveness of Improving The ACD in The Second Stage of The TH&P Model

For a clearer illustration of the process of selecting each line in the second-stage model, taking the scheme of the TH&P model in Table V as an example, the resilience increment of the remaining lines in the 1st iteration of the TH&P model is shown in Fig. 5. We observe lines 5–10, 2–4, and 2–6 have the same highest resilience increment (12.83%) among the 10 lines but different construction costs. In this situation, line 5–10 is chosen as the next hardening line because it has the lowest construction cost.

Then, the top 10 lines in the 2nd iteration after line 5–10 is hardened are shown in Fig. 6 to demonstrate the resilience increment between the two adjacent iterations. By comparing Figs. 5 and 6, it can be found resilience increments of the top 10 lines are generally lower overall after hardening a line. This feature is obvious on some lines, such as lines 1–3 (the resilience increment drops from 12.48% to 4.07%). Since hardening any one line will have an impact on the contributions of the ACDs of the other lines, in this paper, we decided to reinforce only one line instead of multiple lines per iteration in the second-stage model.

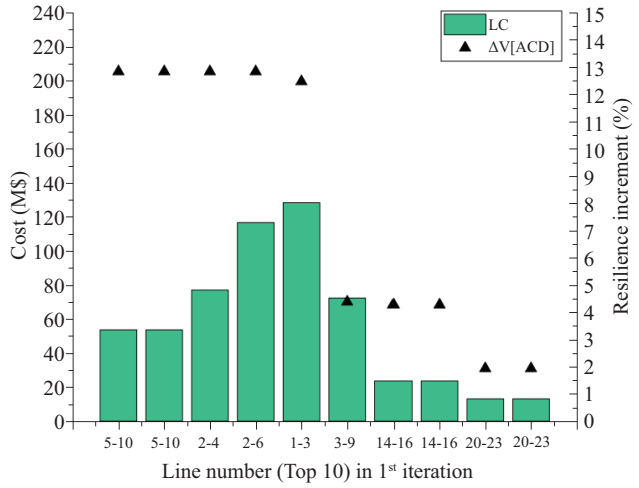

Fig. 5. Resilience increment of the remaining lines in the 1st iteration (top 10).

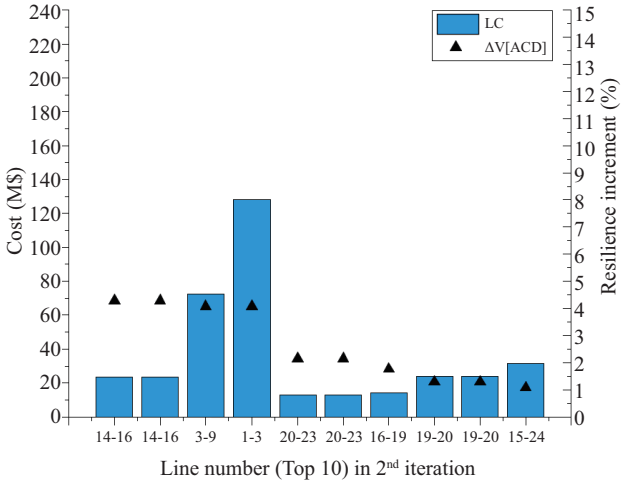

Fig. 6. Resilience increment of the remaining lines in the 2nd iteration (top 10).

3) The Advantages of Collaborative Hardening and Planning Measures

To address the research gap stemming from the combination of transmission HMs and PMs not being fully explored and to illustrate the advantages of the proposed TH&P model in economic terms, a comparison case (C3) is utilized. The core difference between the TH&P model and C3 is shown in Table VI, namely the collaborative or separate implementation of HMs and PMs to meet requirements of normal and damage scenarios.

TABLE VI
TH&P VS. C3

Stage	Aspect	TH&P	C3
First	Resilience measures for scenarios	Hardening and planning for both NS and DS	Planning for NS, hardening for DS
	Aim	Meet the load growth demand of NS and the requirement for V[LSP] for DS	
Second	Resilience measures	Hardening	Hardening
	Aim	Developing the V[ACD] of the scheme obtained in the first stage until V[ACD] meets the target	

The planning results are presented in Table VII, which indicates both the TH&P model and C3 meet the two RAIs' requirements at a certain cost.

TABLE VII
PLANNING SCHEMES OF THE IEEE RTS-24 SYSTEM

Aspect		TH&P	C3
PC (M$)		179.4	158.2
HC (M$)		851.9	874.3
OC (M$)		1907.6	1985.3
LSC (M$)		0	0
TC (M$)		2938.9	3017.8
V[LSP] (%)		100	100
V[ACD] (%)		100	100
Planning	Same	1-5, 5–10, 6–10, 14–16, 16–17, 17–18	
	Difference	11-14	–
Hardening	Same	1-2, 1–5, 4–9, 6–10(2), 7–8(2), 8–9, 11–14, 12–13, 12–23, 14–16, 15–21, 16–19, 17–18, 17–22, 20–23	
	Difference	3-9, 5–10, 11–14, 13–23, 15–16	1-3, 2–4, 15–24

In comparison, the proposed TH&P model saves \$78.9 M in TC (approximately 2.6%). Additionally, the TCs of PMs and HMs are almost the same for the two models (for the TH&P model, (PC+HC) = \$1031.3 M, while for C3, (PC+HC) = \$1032.5 M). Thus, the cost savings are mainly on the operational side, which is due to consideration of the collaborative capacity of HMs and PMs, resulting in a more rational transmission network structure.

To further illustrate the process of effectively developing V[ACD] through the second stage of the proposed model, the changes in TC and V[ACD] in each iteration are shown together in Fig. 7. Part (a) is used as an example for analysis.

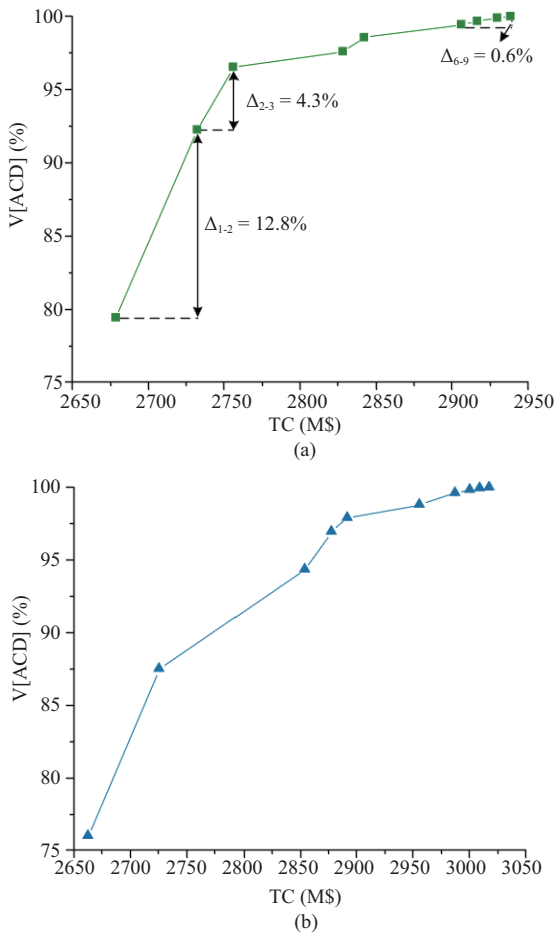

Fig. 7. The changes in the TC and V[ACD] in each iteration. (a) TH&P. (b) C3.

In the 1st iteration, the TC of the planning scheme obtained in the first stage is \$2678.9 M, and V[ACD] is 79.4%. V[ACD] does not meet the requirements (in this paper, V[ACD] needs to be 100%; in practice, different V[ACD] values can be set based on different situations). Therefore, the second-stage model is initiated. After calculating the resilience increment of the remaining lines (not hardened), line 5–10 is selected as the next line to be enhanced. Continuing to the 2nd iteration, the TC increases to \$2732.5 M, and V[ACD] is 92.2%. At the 9th iteration, V[ACD] reaches 100%, and at that point, the TC reaches \$2938.8 M. From the V[ACD] curve in Fig. 7(a), the resilience improvement is most significant in the first few iterations (1st–2nd iterations) and gradually decreases in each subsequent iteration. Therefore, a smaller V[ACD] (e.g., 95%) can be set to properly consider the cost–benefit issue, and the remaining 5% of the requirement can be addressed through post-disaster resilience measures (e.g., response measures, but this is not the focus of this paper).

4) Maximum Resilience Enhancement Scheme of The TH&P Model Under Different Budgets

The proposed TH&P model can not only effectively obtain hardening and planning schemes meeting the requirements of the two RAIs but also provide the maximum resilience improvement strategies for different budgets. The sensitivity analysis results are shown in Table VIII, and we observe

TABLE VIII
MAXIMUM RESILIENCE VALUES AT DIFFERENT BUDGETS

Budget (M$)	TC (M$)	V[LSP] (%)	Maximum V[ACD] (%)
2700	2691	100	81.35
2750	2745.6	100	94.40
2800	2793.8	100	97.49
2850	2842.5	100	98.56
2900	2891.8	100	99.35

that V[ACD] improves as the budget increases, with marginal utility. This means return on the same cost investment up-front is higher than those of later investments. In addition, the increase in the per unit budget (\$50 M) has a greater impact on improvement in V[ACD] when the budget is less than \$2750 M. Specifically, when the budget increases from \$2700 M to \$2750 M, the maximum V[ACD] increases by 13.05%; however, the next \$50 M budget increment (from \$2750 M to \$2800 M) increases V[ACD] by only 3.09%. Therefore, in practice, a reasonable V[ACD] can be set in consideration of the cost–benefit ratio.

5) TH&P Schemes with Different Wind Farm Capacities

Wind power generators in the path of a hurricane are assumed to shut down to avoid destruction by excessive wind speeds. To further study the impact of increased installed wind power capacity (WPC) on hardening and planning schemes, four comparison scenarios are constructed with total WPCs of 0 MW, 600 MW, 1200 MW, and 2400 MW. The planning results are presented in Fig. 8. (HC1 and HC2 represent the hardening costs of the first and second stages, respectively). Fig. 8 shows TC decreases as the WPC increases, with the main reduction being in OCs (the green part in Fig. 8). For example, when the installed WPC increases from 0 MW to 2400 MW, the TC decreases from \$3435.6 M to \$2938.8 M (approximately 14.5%). In particular, the OC is reduced from \$2331.8 M to \$1907.6 M, which is due to replacement of the output of the thermal generator with wind power. Moreover, the PC of the scenario WPC = 1200 MW is less than the other two scenarios (WPC = 2400 MW and WPC = 0 MW) because when considering large or not installed WPCs, new lines are generally required to ensure the outputs of thermal and wind power.

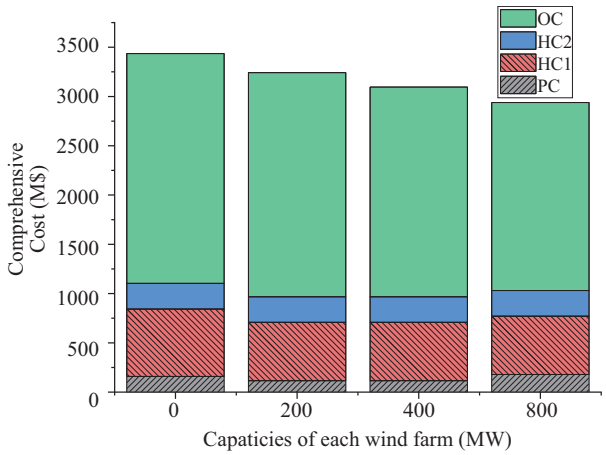

Fig. 8. Planning results with different capacities of each wind farm.

B. Two-area IEEE RTS-1996

The modified two-area IEEE RTS-1996 is used as a large system to show the effectiveness of the proposed TH&P model. This case has two areas and 71 transmission corridors. Total load and generator capacity are 5700 MW and 6810 MW, respectively, and the original information of each area is the same as the IEEE RTS-24. The following modifications are made: the thermal power capacity and load demand are increased to 1.5 times their original values. Corridors 7–8 and 31–32 add a new line. Wind farms are connected to buses 5, 8, and 19 for area 1 and to buses 29, 32, and 43 for area 2 with the same initial capacity of 800 MW.

The states of the corridor under typical hurricane damage scenarios and the geographical location map of the two-area IEEE RTS-1996 are introduced in the appendix (Table AI and Fig. A1). According to Table AI, no transmission lines in area 2 are destroyed in the four typical damage scenarios because they are far away from the hurricane. One of the three tie lines between two areas is destroyed in some scenarios because it is closest to the hurricane landfall, where the hurricane intensity is higher.

Under the simulated hurricane, the TC of the TH&P model satisfies the requirements of both RAIs is \$3443.5 M. Compared to C1, the cost increment is approximately 8.8%, and V[ACD] increases by 12.3%. Compared with C2, the TC of the TH&P model is reduced by approximately 11.3%, and the V[LSP] of the TH&P model increases by approximately 1.4%. Compared to C3, cost savings are approximately 2.1%. The specific resilience enhancement scheme is shown in the appendix. The results of the maximum resilience value for different budgets are presented in Table IX, and we observe when the budget increases from \$3150 M to \$3200 M, the improvement in the maximum V[ACD] is most significant, approximately 7.69%. Moreover, the impact of the subsequent budget increments (\$50 M) gradually decreases. Additionally, when the installed WPC increases from 0 MW to 4800 MW, the TC of the scheme meeting requirements of the two RAIs decreases from \$4977.7 M to \$3443.5 M, almost 30.8%.

TABLE IX
MAXIMUM RESILIENCE VALUES AT DIFFERENT BUDGETS

Budget (M$)	TC (M$)	V[LSP] (%)	Maximum V[ACD] (%)
3150	3149.4	100	87.95
3200	3192.5	100	95.64
3250	3249.4	100	98.77
3300	3293.2	100	99.33
3350	3349.7	100	99.44
3400	3399	100	99.67

VI. CONCLUSION

This paper proposes a novel two-stage TH&P model to meet the load growth demand of normal scenarios and the resilience requirements of hurricane-induced damage scenarios. The proposed TH&P model is verified on a modified IEEE RTS-24 and two-area IEEE reliability test system-1996.

Simulation results reveal 1) resilient PMs and HMs can be taken on the transmission system effectively and economically with the proposed model. 2) The proposed model can also provide a maximized resilience enhancement strategy with different budgets, which can help transmission planners make decisions in the case of inadequate budgets. 3) Increasing the installed capacity of wind power can effectively reduce the OC and thus further reduce the TC.

In practical applications, when transmission systems in hurricane-prone coastal areas need to meet the requirements of load growth with extra construction, strengthening methods such as grounding overhead lines and employing more robust materials can be deployed. Thus, a powerful tool is presented for network owners to expand the existing power system with maximum resilience with respect to a limited budget.

This work has some limitations. It considers only direct line failures caused by hurricanes, ignoring subsequent cascading failures. In future studies, we can analyze the fault propagation process after the first failure of a line to obtain a more realistic fault scenario. Moreover, we will further increase number of considered hurricanes based on practical data to make the resilience enhancement scheme resilient to more hurricanes.

APPENDIX

TABLE AI
TYPICAL HURRICANE DAMAGE SCENARIOS FOR THE TWO-AREA IEEE RTS

C_{num}	fb	tb	State				C_{num}	fb	tb	State			
			1	2	3	4				1	2	3	4
1	1	2			⋆		42	25	29				
2	1	3	⋆	⋆	⋆	⋆	43	26	28				
3	1	5			⋆	⋆	44	26	30				
4	2	4	⋆	⋆	⋆	⋆	45	27	33				
5	2	6	⋆	⋆	⋆	⋆	46	27	48				
6	3	9		⋆	⋆	⋆	47	28	33				
7	3	24					48	29	34				
8	4	9		⋆	⋆	⋆	49	30	34				
9	5	10		⋆	⋆	⋆	50+51	31	32				
10	6	10	⋆	⋆	⋆	⋆	52	32	33				
11+12	7	8	⋆		⋆	⋆	53	32	34				
13	8	9	⋆	⋆	⋆	⋆	54	33	35				
14	8	10	⋆	⋆	⋆	⋆	55	33	36				
15	9	11					56	34	35				
16	9	12					57	34	36				
17	10	11					58	35	37				
18	10	12					59	35	38				
19	11	13	⋆	⋆	⋆	⋆	60	36	37				
20	11	14	⋆	⋆		⋆	61	36	47				
21	12	13	⋆	⋆	⋆	⋆	62	37	47				
22	12	23		⋆	⋆	⋆	63	38	40				
23	13	23				⋆	64	39	40				
24	14	16					65+66	39	45				
25	15	16					67	39	48				
26+27	15	21	⋆			⋆	68	40	41				
28	15	24					69	40	43				
29	16	17					70	41	42				
30	16	19					71	41	46				
31	17	18					72+73	42	45				
32	17	22				⋆	74+75	43	44				
33+34	18	21					76+77	44	47				
35+36	19	20					78	45	46				
37+38	20	23			⋆		79	23	41				
39	21	22					80	13	39				
40	25	26					81	7	27	⋆		⋆	⋆
41	25	27											

⋆ indicates that a corridor is damaged under the damage scenarios.

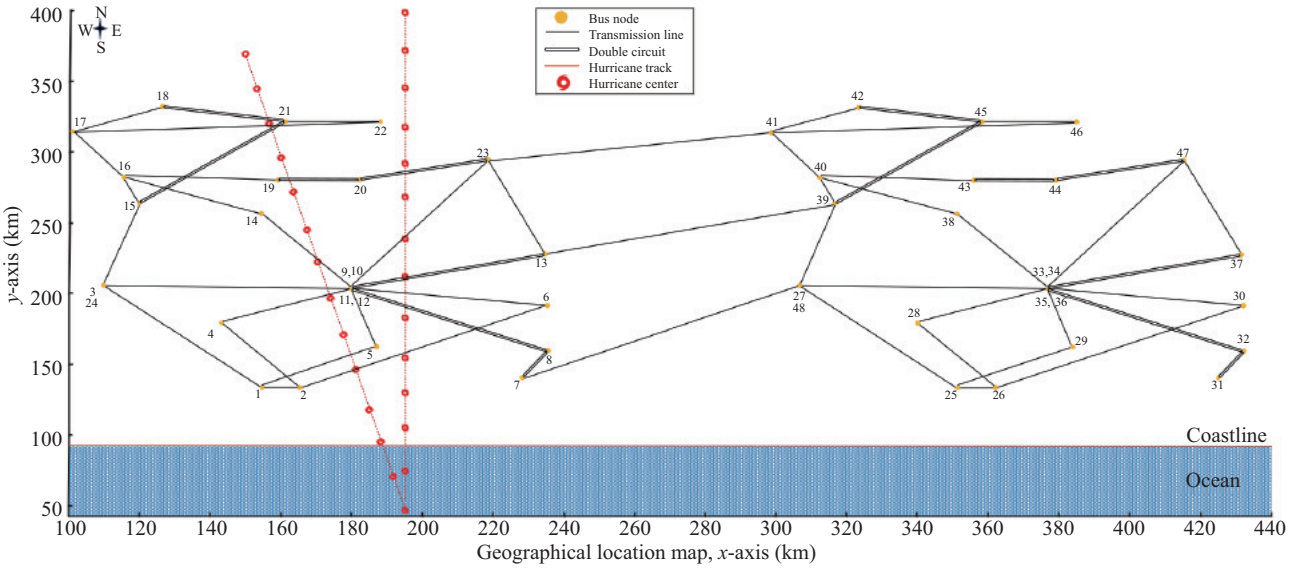

Fig. A1. Two-area IEEE reliability test system-1996 under two simulated hurricanes.

TABLE AII
PLANNING SCHEMES OF THE IEEE RTS-24 SYSTEM

REM	Aspect	TH&P	C1	C2
Planning	Same	1-5, 5–10, 6–10, 14–16, 16–17, 17–18		
	Difference	11-14	11-14	–
Hardening	Same	1-5, 4–9, 6–10, 7–8, 8–9, 11–14, 12–23, 15–21		
	Difference	1-2, 3–9, 5–10, 6–10, 7–8, 11–14, 12–13, 13–23, 14–16, 15–16, 16–19, 17–18, 17–22, 20–23	1-2, 6–10, 7–8, 11–14, 12–13, 13–23	1-3, 3–9, 11–13, 15–24, 16–19, 17–18, 17–22, 20–23

TABLE AIII
PLANNING SCHEMES OF THE TWO-AREA IEEE RTS-1996 SYSTEM

REM	Aspect	TH&P	C1	C2
Planning	Same	1-5, 6–10, 14–16, 16–17, 17–18		
	Difference	25-29, 38–40, 40–41	25-29, 38–40, 40–41	5-10
Hardening	Same	1-5, 4–9, 6–10, 7–8, 7–27, 11–14, 15–21, 20–23		
	Difference	1-2, 3–9, 5–10, 6–10, 8–9, 12–13, 13–23, 14–16, 16–17, 16–19, 17–18, 17–22	1-2, 6–10, 8–9, 12–13	1-3, 3–9, 11–13, 13–23, 13–39, 15–24, 16–19, 18–21, 21–22

REFERENCES

[1] A. B. Smith and R. W. Katz, "US billion-dollar weather and climate disasters: data sources, trends, accuracy and biases," *Natural Hazards*, vol. 67, no. 2, pp. 387–410, Feb. 2013.

[2] X. R. Yang, L. Lü, L. X. Xu, Y. B. Liu, C. Z. Zhu, Q. Xiong, and Y. Li, "Probabilistic security evaluation of urban transmission considering elastic margin," *Power System Technology*, vol. 43, no. 2, pp. 705–713, Feb. 2019.

[3] M. Mahzarnia, M. P. Moghaddam, P. T. Baboli, and P. Siano, "A review of the measures to enhance power systems resilience," *IEEE Systems Journal*, vol. 14, no. 3, pp. 4059–4070, Sep. 2020.

[4] W. Zhang, D. Rui, W. Wang, Y. Guo, Z. Jing and W. Tang, "Cyber-physical resilience enhancement for power transmission systems with energy storage systems," *CSEE Journal of Power and Energy Systems*, doi: 10.17775/CSEEJPES.2022.07570.

[5] E. Hossain, S. Roy, N. Mohammad, N. Nawar, and D. R. Dipta, "Metrics and enhancement strategies for grid resilience and reliability during natural disasters," *Applied Energy*, vol. 290, pp. 116709, May 2021.

[6] A. Bagheri, C. Y. Zhao, F. Qiu, and J. H. Wang, "Resilient transmission hardening planning in a high renewable penetration era," *IEEE Transactions on Power Systems*, vol. 34, no. 2, pp. 873–882, Mar. 2019.

[7] F. Hasanzad and H. Rastegar, "Application of optimal hardening for improving resilience of integrated power and natural gas system in case of earthquake," *Reliability Engineering & System Safety*, vol. 223, pp. 108476, Jul. 2022.

[8] H. Wang, K. Hou, J. B. Zhao, X. D. Yu, H. J. Jia, and Y. F. Mu, "Planning-Oriented resilience assessment and enhancement of integrated electricity-gas system considering multi-type natural disasters," *Applied Energy*, vol. 315, pp. 118824, Jun. 2022.

[9] K. Jalilpoor, A. Oshnoei, B. Mohammadi-Ivatloo, and A. Anvari-Moghaddam, "Network hardening and optimal placement of microgrids to improve transmission system resilience: A two-stage linear program," *Reliability Engineering & System Safety*, vol. 224, pp. 108536, Aug. 2022.

[10] M. Panteli, D. N. Trakas, P. Mancarella, and N. D. Hatziargyriou, "Power systems resilience assessment: hardening and smart operational enhancement strategies," *Proceedings of the IEEE*, vol. 105, no. 7, pp. 1202–1213, Jul. 2017.

[11] Y. Yuan, H. Zhang, H. Z. Cheng, and Z. Wang, "Resilience-oriented transmission expansion planning with optimal transmission switching under typhoon weather," *CSEE Journal of Power and Energy Systems*, vol. 10, no. 1, pp. 129–138, Jan. 2024, doi: 10.17775/CSEEJPES.2021.07840.

[12] B. Zhang, P. Dehghanian, and M. Kezunovic, "Optimal allocation of PV generation and battery storage for enhanced resilience," *IEEE Transactions on Smart Grid*, vol. 10, no. 1, pp. 535–545, Jan. 2019.

[13] M. Shivaie, M. Kiani-Moghaddam, and P. D. Weinsier, "Resilience-based tri-level framework for simultaneous transmission and substation expansion planning considering extreme weather-related events," *IET Generation, Transmission & Distribution*, vol. 14, no. 16, pp. 3310–3321, Aug. 2020.

[14] M. Moradi-Sepahvand, T. Amraee, and S. S. Gougheri, "Deep learning based hurricane resilient coplanning of transmission lines, battery energy storages, and wind farms," *IEEE Transactions on Industrial Informatics*,

vol. 18, no. 3, pp. 2120–2131, Mar. 2022.
[15] H. Ranjbar, S. H. Hosseini, and H. Zareipour, "Resiliency-Oriented planning of transmission systems and distributed energy resources," *IEEE Transactions on Power Systems*, vol. 36, no. 5, pp. 4114–4125, Sep. 2021.
[16] J. H. Yan, B. Hu, K. G. Xie, J. J. Tang, and H. M. Tai, "Data-Driven transmission defense planning against extreme weather events," *IEEE Transactions on Smart Grid*, vol. 11, no. 3, pp. 2257–2270, May 2020.
[17] R. Yang and Y. Li, "Resilience assessment and improvement for electric power transmission systems against typhoon disasters: A data-model hybrid driven approach," *Energy Reports*, vol. 8, pp. 10923–10936, Nov. 2022.
[18] H. Hamidpour, S. Pirouzi, S. Safaee, M. Norouzi, and M. Lehtonen, "Multi-objective resilient-constrained generation and transmission expansion planning against natural disasters," *International Journal of Electrical Power & Energy Systems*, vol. 132, pp. 107193, Nov. 2021.
[19] T. Ding, M. Qu, Z. K. Wang, B. Chen, C. Chen, and M. Shahidehpour, "Power system resilience enhancement in typhoons using a three-stage day-ahead unit commitment," *IEEE Transactions on Smart Grid*, vol. 12, no. 3, pp. 2153–2164, May 2021.
[20] T. Y. Zhao, H. J. Zhang, X. C. Liu, S. H. Yao, and P. Wang, "Resilient unit commitment for day-ahead market considering probabilistic impacts of hurricanes," *IEEE Transactions on Power Systems*, vol. 36, no. 2, pp. 1082–1094, Mar. 2021.
[21] S. Liu, Y. Li, X. Liu, T. Zhao and P. Wang, "Resilient Power Systems Operation with Offshore Wind Farms and Cloud Data Centers," *CSEE Journal of Power and Energy Systems*, vol. 9, no. 6, pp. 1985–1998, November. 2023.
[22] X. T. Sun, H. P. Xie, Z. H. Bie, and G. F. Li, "Restoration of high-renewable-penetrated distribution systems considering uncertain repair workloads," *CSEE Journal of Power and Energy Systems*, to be published, doi: 10.17775/CSEEJPES.2021.06500.
[23] W. X. Liu, Y. H. Wang, Q. X. Shi, Q. Yao, and H. Y. Wan, "A multi-stage restoration strategy to enhance distribution system resilience with improved conditional generative adversarial nets," *CSEE Journal of Power and Energy Systems*, to be published, doi: 10.17775/CSEEJPES.2021.09080.
[24] R. Tao, D. M. Zhao, H. X. Wang, and X. Xia, "Multi-stage defender-attacker-defender model for distribution system resilience enhancement in ice storms with line hardening, mobile device and repair crew dispatching," *CSEE Journal of Power and Energy Systems*, vol. 9, no. 3, pp. 1103–1118, May 2023, doi: 10.17775/CSEEJPES.2021.05510.
[25] W. Tang, Z. Q. Wang, L. Zhang, B. Zhang, J. Liang, K. Y. Liu, and W. X. Sheng, "Optimal allocation strategy of electric EPSVs and hydrogen fuel cell EPSVs balancing resilience and economics," *CSEE Journal of Power and Energy Systems*, to be published, doi: 10.17775/CSEEJPES.2021.05430.
[26] M. E. Batts, E. Simiu, and L. R. Russell, "Hurricane wind speeds in the United States," *Journal of the Structural Division*, vol. 106, no. 10, pp. 2001–2016, Oct. 1980
[27] P. J. Vickery, "Simple empirical models for estimating the increase in the central pressure of tropical cyclones after landfall along the coastline of the United States," *Journal of Applied Meteorology and Climatology*, vol. 44, no. 12, pp. 1807–1826, Dec. 2005.
[28] R. Rocchetta, E. Zio, and E. Patelli, "A power-flow emulator approach for resilience assessment of repairable power grids subject to weather-induced failures and data deficiency," *Applied Energy*, vol. 210, pp. 339–350, Jan. 2018.
[29] Y. Z. Wang, C. Chen, J. H. Wang, and R. Baldick, "Research on resilience of power systems under natural disasters-A review," *IEEE Transactions on Power Systems*, vol. 31, no. 2, pp. 1604–1613, Mar. 2016.
[30] X. N. Liu, K. Hou, H. J. Jia, J. B. Zhao, L. Mili, X. L. Jin, and D. Wang, "A planning-oriented resilience assessment framework for transmission systems under typhoon disasters," *IEEE Transactions on Smart Grid*, vol. 11, no. 6, pp. 5431–5441, Nov. 2020.
[31] X. Z. Song, Z. Wang, D. Q. Gan, and J. J. Qiu, "Transient stability risk assessment of power grid under typhoon weather," *Power System Protection and Control*, vol. 40, no. 24, pp. 1–8, Dec. 2012.
[32] H. J. Zhang, L. Cheng, S. H. Yao, T. Y. Zhao, and P. Wang, "Spatial–Temporal reliability and damage assessment of transmission networks under hurricanes," *IEEE Transactions on Smart Grid*, vol. 11, no. 2, pp. 1044–1054, Mar. 2020.
[33] Probability Methods Subcommittee, "IEEE reliability test system," *IEEE Transactions on Power Apparatus and Systems*, vol. PAS-98, no. 6, pp. 2047–2054, Nov. 1979.
[34] C. Grigg, P. Wong, P. Albrecht, R. Allan, M. Bhavaraju, R. Billinton, Q. Chen, C. Fong, S. Haddad, S. Kuruganty, W. Li, R. Mukerji, D. Patton, N. Rau, D. Reppen, A. Schneider, M. Shahidehpour, and C. Singh, "The IEEE reliability test system-1996. A report prepared by the reliability test system task force of the application of probability methods subcommittee," *IEEE Transactions on Power Systems*, vol. 14, no. 3, pp. 1010–1020, Aug. 1999.
[35] P. J. Vickery and L. A. Twisdale, "Wind-field and filling models for hurricane wind-speed predictions," *Journal of Structural Engineering*, vol. 121, no. 11, pp. 1700–1709, Nov. 1995.
[36] Y. Chen, S. Y. Wang, B. Chen, T. S. Xu, C. Yu, and J. L. Yu, "Evaluation of the failure probability of power transimmission corridors during typhoons using digital elevation information," *Power System Technology*, vol. 42, no. 7, pp. 2295–2302, Jul. 2018.
[37] M. Panteli, C. Pickering, S. Wilkinson, R. Dawson, and P. Mancarella, "Power system resilience to extreme weather: fragility modeling, probabilistic impact assessment, and adaptation measures," *IEEE Transactions on Power Systems*, vol. 32, no. 5, pp. 3747–3757, Sep. 2017.
[38] H. Zhang, H. Z. Cheng, L. Liu, S. X. Zhang, Q. Zhou, and L. Jiang, "Coordination of generation, transmission and reactive power sources expansion planning with high penetration of wind power," *International Journal of Electrical Power & Energy Systems*, vol. 108, pp. 191–203, Jun. 2019.
[39] H. Zhang, H. Z. Cheng, J. P. Zhang, L. Liu, Y. Zeng, and J. Z. Lu, "Generation and transmission expansion planning considering $N-1$ security constraints with high penetration of wind power," *Proceedings of the CSEE*, vol. 38, no 20, pp. 5929–5936, Oct. 2018.

Jing Zhou received the B.S. degree in Electrical Engineering from Southwest Jiaotong University, Sichuan, China, in 2017. He is currently pursuing the Ph.D. degree in Electrical Engineering at Shanghai Jiao Tong University, Shanghai, China. His research interests include power system planning.

Heng Zhang received the Ph.D. degree in Electrical Engineering, Shanghai Jiao Tong University, Shanghai, China, in 2019. Now, he is an Associate Researcher in Shanghai Jiao Tong University. His main research interests are power market, and power system planning.

Haozhong Cheng received the Ph.D. degree in Power Systems from Shanghai Jiao Tong University, Shanghai, China, in 1998. He is current a Professor in School of Electronic Information and Electrical Engineering, Shanghai Jiao Tong University. His research interests are mainly power system planning, operation, and deregulation.

Shenxi Zhang received the B.S. degree in Electrical Engineering from Hohai University, Nanjing, China, in 2011. He received the Ph.D. degree in Electrical Engineering from Shanghai Jiao Tong University, Shanghai, China, in 2016. He is currently an Associate Researcher with Shanghai Jiao Tong University. His main research interests include power system optimization, renewable generation, and integrated energy system.

Lu Liu received the B.S. and M.S. degrees in Electrical Engineering from Wuhan University, Wuhan, China, in 2006 and 2008, respectively, and received the Ph.D. degree in Electrical Engineering from Shanghai Jiao Tong University, Shanghai, China, in 2012. Currently, she is working as an Associate Researcher with the Key Laboratory of Control of Power Transmission and Conversion, Ministry of Education, Shanghai Jiao Tong University. Her research interests include transmission network planning and assessment, co-ordination planning of transmission and distribution networks.

Zheng Wang is a senior engineer of State Grid East China Branch. His research interests are mainly power system planning and operation.

Xiaohu Zhang is a senior engineer of State Grid East China Branch. His research interests are mainly power system planning.